



POLİTEKNİK DERGİSİ

JOURNAL of POLYTECHNIC

ISSN: 1302-0900 (PRINT), ISSN: 2147-9429 (ONLINE)

URL: <http://dergipark.org.tr/politeknik>



Weldability of haynes 188 cobalt based superalloy and AISI 316L austenitic stainless steel

Haynes 188 kobalt esaslı süperalaşım ile AISI 316L ostenitik paslanmaz çeliğin kaynak edilebilirliği

Yazar(lar) (Author(s)): Samet NOHUTÇU¹, Ramazan KAÇAR², Hayriye ERTEK EMRE³

ORCID¹: 0000-0002-2600-3993

ORCID²: 0000-0002-3903-1838

ORCID³: 0000-0002-8218-037X

To cite to this article: Nohutçu S., Kaçar R. and Ertek H. E., “Weldability of haynes 188 cobalt based superalloy and AISI 316L austenitic stainless steel”, *Journal of Polytechnic*, 27(3): 995-1004, (2024).

Bu makaleye şu şekilde atıfta bulunabilirsiniz: Nohutçu S., Kaçar R. ve Ertek H. E., “Haynes 188 kobalt esaslı süperalaşım ile AISI 316L ostenitik paslanmaz çeliğin kaynak edilebilirliği”, *Politeknik Dergisi*, 27(3): 995-1004, (2024).

Erişim linki (To link to this article): <http://dergipark.org.tr/politeknik/archive>

DOI: 10.2339/politeknik.1231345

Weldability of Haynes 188 Cobalt Based Superalloy and AISI 316L Austenitic Stainless Steel

Highlights

- ❖ Cobalt Base Superalloy
- ❖ Dissimilar Metals Welding (Superalloy- Austenitic stainless steel)
- ❖ Autogenous Welding by Force TIG welding Machine
- ❖ Mechanical Properties and Microstructural Examinations

Graphical Abstract

The study aims to investigate the weldability of the Haynes 188 - AISI 316L couple, as supplied, automatically with the Force TIG welding machine, without a weld groove, and without using any additional metal (autogenously). For this purpose, the strength and hardness of the dissimilar welded sample were determined, and its microstructure was evaluated in detail.

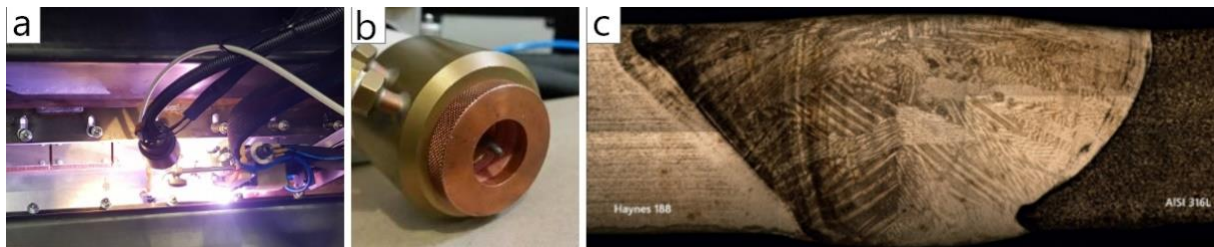


Figure a) Welding process, **b)** Force TIG welding machine torch, **c)** Macrostructures of the welded samples.

Aim

Unlike the conventional TIG welding method, this study investigated the autogenous weldability of Haynes 188 superalloy and AISI 316L austenitic stainless-steel couple with Force TIG welding machine.

Design & Methodology

The mechanical properties of dissimilar metals joint obtained by optimum welding parameters determined with pre-experimental studies, are investigated. For this purpose, a tensile test was carried out and compared with the base metal strengths. In addition, fracture characteristic of the tensile test specimens was evaluated. Hardness measurements of the weldment were carried out. The microstructure of dissimilar welded samples was examined, and EDS analyzes were carried out for determining precipitates.

Originality

The joining of Haynes 188 Cobalt Based Superalloy and AISI 316L Austenitic Stainless Steel dissimilar materials couple with Force TIG welding machine without using filler metal was carried out for the first time in the literature in this study.

Findings

The strength of dissimilar metals weldment, autogenously welded with a Force TIG welding machine, was found higher than that of AISI 316L austenitic stainless steel and lower than that of Haynes 188 superalloy. The strength of the welded joints of dissimilar metals is desired to be higher than the lowest strength material forming the weldment.

Conclusions

The results show that the Haynes188 – AISI 316L couple has been successfully autogenously joined with a Force TIG welding machine without a weld groove.

Declaration of Ethical Standards

The authors of this article declare that the materials and methods used in this study do not require ethical committee permission and legal-special permission.

Weldability of Haynes 188 Cobalt Based Superalloy and AISI 316L Austenitic Stainless Steel

(Bu çalışma ICMATSE 2022 konferansında sunulmuştur. / This study was presented at ICMATSE 2022 conference.)

Araştırma Makalesi / Research Article

Samet NOHUTÇU*, Ramazan KAÇAR, Hayriye Ertek EMRE

Teknoloji Fakültesi, İmalat Mühendisliği Bölümü, Karabük Üniversitesi, Türkiye

(Geliş/Received : 09.01.2023 ; Kabul/Accepted : 23.01.2023 ; Erken Görünüm/Early View : 09.03.2023)

ABSTRACT

Because of their high temperature and oxidation resistance, similar and dissimilar metal welding is needed in producing gas turbine and rocket engine parts, in which cobalt-based superalloys are also used. The fusion welding methods such as gas tungsten arc welding (TIG), Laser welding (LW), Electron beam welding (EBW), and Plasma arc welding (PAW) are widely used for dissimilar metals welding applications. Weld discontinuity such as solidification cracks and liquefaction cracks can occur in the weldment. One way to overcome these problems is to use a low heat input in the welding process. Force TIG welding machine, which has been developed in recent years, allows automatic welding with its integrated systems. Thus, it provides the opportunity to obtain the heat input homogeneously and to perform autogenous welding with its control of the welding parameters. The study aims to investigate the weldability of the Haynes 188 – AISI 316L couple, as supplied, automatically with the Force TIG welding machine, without opening the weld groove, and without using any filler metal (autogenously). For this purpose, the strength and hardness of the dissimilar welded sample were determined, and its microstructure was evaluated in detail.

Keywords: Haynes 188, AISI 316L, weldability, microstructure and mechanical properties.

Haynes 188 Kobalt Esaslı Süperalaşım ile AISI 316L Ostenitik Paslanmaz Çeliğin Kaynak Edilebilirliği

ÖZ

Kobalt esaslı süper esaslı süperalaşımın da kullanıldığı gaz türbini ve roket motor parçalarının üretiminde, yüksek sıcaklık ve oksidasyon dirençleri nedeniyle benzer ve benzer olmayan metallerin kaynağına ihtiyaç duyulmaktadır. Gaz tungsten ark kaynağı (TIG), Lazer kaynağı (LW), Elektron ışını kaynağı (EBW) ve Plazma ark kaynağı (PAW) gibi ergitme kaynak işlemleri, benzer olmayan metallerin kaynak uygulamaları için yaygın olarak kullanılmaktadır. Kaynaklı birleştirmelerde katılaşma ve sıvılaşma çatlakları gibi kaynak kusurları oluşabilir. Bu sorunların üstesinden gelmenin bir yolu, kaynak işleminde düşük ısı girdisi kullanmaktır. Son yıllarda geliştirilen Force TIG kaynak makinesi entegre edildiği sistemler ile otomatik kaynak yapmaya imkân vermektedir. Böylece ısı girdisini homojen olarak elde etme ve kaynak parametreleri üzerindeki kontrolü ile otojen kaynak yapma olanağı sağlar. Çalışmada; Haynes 188-AISI 316L çiftinin tedarik edildiği şekliyle Force TIG kaynak makinesi ile otomatik olarak, kaynak ağızı açılmadan ve herhangi bir ilave metal kullanılmadan (otojen olarak) kaynaklanabilirliğinin araştırılması amaçlanmıştır. Bu amaçla, farklı cins malzeme kaynaklı numunenin dayanımı, sertliği belirlenmiş ve mikroyapısı detaylı olarak değerlendirilmiştir.

Anahtar Kelimeler: Haynes 188, AISI 316L, kaynak edilebilirlik, mikroyapı ve mekanik özellikler.

1. INTRODUCTION

Austenitic stainless steels are a highly preferred material type for use over wide temperature ranges. They combine ductility, strength, toughness, good corrosion resistance and well weldability [1]. Austenitic stainless steels have good weldability. AISI 316L steel, which is an important member of this family, also has better weldability due to its lower carbon content in its composition [2,3]. Superalloys are materials with high mechanical strength, creep and also good corrosion resistance due to solid solution and precipitation hardening treatments [4].

The basic elements in superalloys are usually nickel and cobalt. In addition, it may contain aluminum, chromium, iron, molybdenum, titanium and tungsten [5]. Haynes 188 is a cobalt-based superalloy and it is generally used in the aerospace and energy fields, especially in gas turbine engines [5].

Welding of dissimilar metals is frequently used in industrial applications, in many fields, such as the aerospace industry, petrochemistry, chemistry and marine, power plants and vehicle production due to its economic advantages [6]. One of the metals primarily used for dissimilar welding applications is stainless steel [7]. Dissimilar metals joining are very important during the production and assembly of both simple and complex shaped parts to reduce innovation and machining costs. Factors such as increased efficiency, performance and

*Sorumlu Yazar (Corresponding Author)
e-posta : sametohutcu@karabuk.edu.tr

low cost in turbine engines increase the application of superalloys, which can show good strength at high temperatures [8]. Superalloys, which have critical applications in different fields such as energy, gas turbine engine and rocket engine parts, must be welded together with similar and dissimilar metals. Gas shielded arc welding method such as TIG welding is the most common joining method of superalloys [9]. Alloys used at high temperatures are often difficult to weld. The weld defects such as solidification cracks in the melting region of the welded sample and liquefaction cracks in the heat affected zone, (HAZ), can occur. The low heat input is to be used as a solution to these problems. The Force TIG welding machine, which has been developed in recent years, draws attention with its integrated equipment, allowing semi-automatic or fully automatic welding, and providing homogeneous low heat input to the welding zone with its high energy density. It also offers the possibility of autogenous welding on thick-section metals without a weld groove. In the literature, there are fewer studies on the weldability of cobalt-based superalloys with a fusion welding method compared to nickel and iron-based superalloys. The reason for this is thought to be the higher production cost of cobalt-based superalloys and the higher preference of nickel-based superalloys in aerospace applications. Ahmet GN et al. [7] investigated dissimilar metals weldability of duplex stainless steel and Ni-based Inconel 625 superalloy by laser welding. In terms of their extensive structure-property correlation, they suggest that laser welding can be used successfully in joining the mentioned dissimilar metals [7]. Hejrjipour et al. [10] investigated the gas tungsten arc weldability of Inconel 718 and AISI 410 steel using various filler metals. In another study, Osobo et al. [11] emphasized that the precipitation of carbide rich in Titanium (Ti) and Molybdenum (Mo) was witnessed due to significant Ti and Mo inter-dendritic liquefaction in the dendritic cavities in the melting zone of the laser welded Haynes 282 alloy. Ramkumar et al. [12] look into the weldability of Inconel 625 and SAF 2205 EBW and reported that liquefaction cracking occurred in the weld metal. The welding of Inconel 625 and AISI 304L couple by EBW was also investigated by

segregation. It is stated that residual stress, liquefaction and solidification cracking may occur in the welding of dissimilar metals, such as superalloy-stainless steel due to the changing mechanical-thermochemical properties in the melting zone and in the HAZ [14]. The selection of filler metal used in welding has also been determined as an essential critical parameter. It is pointed out that the incompatibility between the additional filler metal used and the main metal joined causes a decrease in strength and a decrease in efficiency due to the formation of residual stresses during welding [7].

When the published issues are investigated, it has been emphasized that different types of superalloy-stainless steel joints are performed. However, no study has been found regarding the joining of Haynes 188 superalloy and AISI 316L austenitic stainless steel. Considering the welding problems associated with high heat input and the problems encountered in the supply of additional filler metal, it is aimed to contribute to the studies in the field by examining the autogenous welding with the Force TIG welding machine without weld groove. For this reason, the Haynes 188 – AISI 316L couple was welded with a Force TIG welding machine by pre-experimentally determined optimum welding parameters. To determine the strength of the weldment, tensile test and microhardness measurement was performed. In addition, detailed microstructure and fracture surface examinations of the welded sample were evaluated.

2. MATERIAL and METHOD

2.1. Materials

The chemical components of the commercially available Haynes 188 and AISI 316L alloys was determined and is shared in Table 1.

2.1. Haynes 188 – AISI 316L Welding Process

Dissimilar metals used in the experiment were cut in 720 x 70 x 3.125 mm³ dimensions and prepared for welding. The surfaces were cleaned with sandpaper and acetone before welding. The water-cooled workpiece gripping jaws integrated with the column boom system were used to prevent distortion and axial shift due to the thermal

Table 1. Chemical composition (weight %) of Haynes 188 superalloy and AISI 316L stainless steel.

Elements (Weight %)	Ni	Cr	W	Fe	Mn	Si
Haynes 188	24.57	19.71	14.834	1.856	0.593	0.23
	Al	S	Nb	Mo	Co	
	0.058	0.059	0.045	0.437	Kalan	
AISI 316L	Fe	C	Cr	Ni	Mo	Mn
	68.66	0.019	16.60	10.08	1.98	1.1
	Si	S	P	Al	Cu	Co
	0.56	0.008	0.03	0.005	0.02	0.24

Shakil et al. [13]. The joining failed due to microcrack formation in the weld metal due to Nb, S, and Mo

welding cycle. The workpiece holder system is made of copper. It works on the principle of compressing the

workpieces placed between the base and the upper plate with high pressure in the butt-welding position. Gas protection is also provided under the weld beam using the protective atmosphere channel on the workpiece holder system, which is designed to be under the welding seam. Preliminary experimental studies determined to the optimum welding parameters that provide the desired joint. For joining, EWM brand DC inverter type FT 1002 Force TIG machine with Ø12mm tungsten electrode, providing welding current up to 1000 Ampere was used. The dissimilar metal couple was autogenously welded. A welding torch with a 15L tank capacity and a water-cooling system was used for the welding process. A constant welding speed of 60 cm/min was used for joining. As a shielding gas at a gas flow rate of 22 L/min, 5% hydrogen-95% argon gas mixture protection was provided. Argon gas at 11.5 bar pressure was used to protect the weld root. Welding process, welding machine torch and weldment plate shown in Figure 1 a,b and d respectively

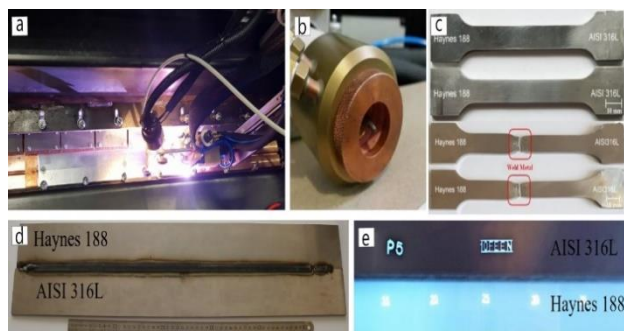


Figure 1. Experimental method a) Welding process, b) Welding machine torch, c) Tensile test specimen, d) Weldment plate, e) X-Ray radiographic examination film of welded Haynes 188 – AISI 316L couple

2.2. Radiographic Inspection Test

Non-destructive testing of post-weld joints was carried out by the radiographic inspection test method. Autogenously welded samples were analyzed with XXGH brand 3005 model X-Ray radiographic inspection device.

2.3. Tensile Test Applied for Weldment

A tensile test was performed to assess the mechanical properties of the dissimilar weldment. The samples were cut on the CNC laser machine in accordance with the TS EN ISO 4136:2012 standard and then machining on the CNC milling machine to improve the surface roughness. The tensile test was performed on a 600kN capacity Zwick/Roell Z600 test device at a crosshead speed of 0.5 mm/min shown in Figure 2a. The macrograph of the prepared tensile specimens and the areas where the specimens fractured after the test are shown in Figure 1c.

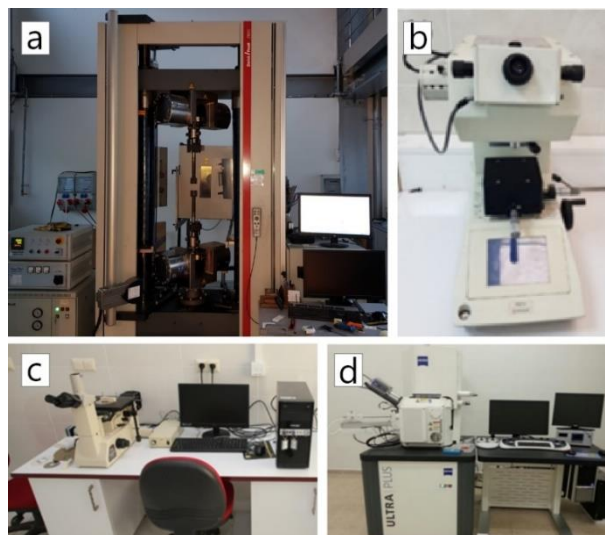


Figure 2. Test devices a) Tensile test machine, b) Vickers microhardness tester, c) Optical microscope, d) SEM and EDS

2.4. Hardness Measurement

The hardness measurement of the joint covering the main metal, HAZ and weld metal was made with the Vickers microhardness tester. A load of 500g was applied to the indenter. Vickers microhardness tester shown in Figure 2b.

2.5. Microstructure Examinations

Cold mounted samples were polished with 1-3 µm diamond solution after grinding with 250-2000 mesh SiC sandpaper for metallographic examination. The 8 ml of hydrochloric acid (HCl) and 8 ml of hydrogen peroxide (H₂O₂) reagent was used for 25 seconds to etching sample. Microstructure examination of welded samples were carried out by using Nikon Epiphot 200 optical microscope. Scanning electron microscope (SEM) examinations of fracture surface were made with Zeiss Ultra Plus brand device and integrated IXRF model EDS. Optical microscope and SEM-EDS shown in Figure 2 c and d respectively.

3. EXPERIMENTAL RESULTS AND EVALUATION

3.1. Radiographic Inspection Result

The non-destructive test result of the dissimilar welded sample was carried out by the radiographic inspection test method is shown in Figure 1e.

According to the radiographic inspection results of Haynes 188 – AISI 316L dissimilar metals joined with a Force TIG welding machine, any weld defects, (discontinuity), in the weldment has not been detected. This indicates that the Haynes 188 – AISI 316L dissimilar metals can be successfully joined with the Force TIG welding machine.

3.2. Tensile Test Results

A tensile test was applied to detect the strength and ductility of the dissimilar welded sample. In addition, tensile tests of AISI 316L and Haynes 188 base metals were also carried out. The mechanical properties data obtained from the base metal and the weldment are shared in Table 2. The mechanical properties data for the welded sample and base, (main), metals were determined by taking the average yield and tensile strengths and elongation. The average stress-strain curves of base metals and Haynes 188 – AISI 316L welded sample is only shown in Figure 3.

Table 2. The mechanical properties of Haynes 188 superalloy, AISI 316L austenitic stainless steel main metals and weldment.

Specimens	Yield Strength (MPa)	Tensile Strength (MPa)	Elongation (%)
Haynes 188	538	1024	77
AISI 316L	285	586.1	61.5
Haynes 188 – AISI 316L - 1	371.5	609.1	27.3
Haynes 188 – AISI 316L - 2	357.4	620.4	28.8
Haynes 188 – AISI 316L (Mean)	364.5	614.8	28.1

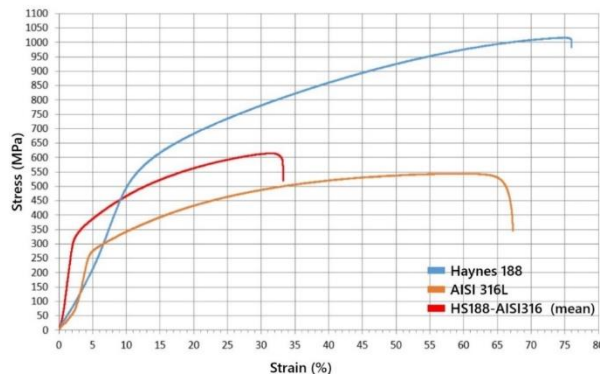


Figure 3. The mean stress-strain curve of Haynes 188 – AISI 316L weldment

As a result of the experiment, the mean ultimate tensile strength, (UTS), of AISI 316L austenitic stainless steel is determined as 586.1MPa, yield strength, (YS) of 285MPa and elongation (EL) amount of 61.5%. The UTS of Haynes 188 superalloy is found to be 1024MPa, YS of 538MPa and EL. 77%. The UTS of Haynes 188 - AISI 316L weldment is determined as 614.8MPa, YS 364.5MPa and % EL amount of 28.1%. It is found that the strength of the autogenously welded dissimilar metals weldment is higher than the strength of AISI 316L stainless steel and lower than the Haynes 188 superalloy. It is desired that the strength of dissimilar metals

weldment should be higher than the lowest strength of the base metals forming the joint. According to the test results, it is concluded that the strength of the weldment is within acceptable ranges. It also results that Haynes 188 - AISI 316L couple can be successfully joined autogenously at butt welding position.

It is seen that the ductility of welded samples is quite low compared to base metals. The reason for this is thought to be the structure, precipitation formations and grain size changes in the weld metal of autogenously welded sample or due to the metallurgical transformation associated with the thermal welding cycle in HAZ. As can be seen from Figure 1b, the tensile test sample is elongated from the AISI 316L base metal side before the fracturing from weld metal.

The fracture surface SEM examinations were carried out on the samples and the fracture surface images are shared in Figure 4.

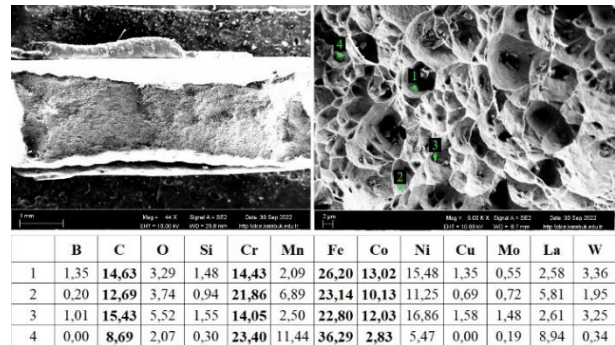


Figure 4. Haynes 188 – AISI 316L weldment fracture surface SEM images and EDS analysis results.

As seen in Figure 4, the fracture of the weld metal is the ductile mode. The apparent decrease in cross section in the fractured surface SEM image, the honeycomb-like structure, pitted surface and dull appearance in the SEM image support this thesis. In addition, it is observed that various precipitates, which are thought to form the fracture initiation, are formed within the pits. According to the point EDS analysis taken from the fractured surface, the decrease in the amount of cobalt, tungsten, molybdenum, and nickel in the structures formed in the pits, but the significant increase in the amount of carbon in the composition can be shown as evidence of the presence of precipitates. It is presumably metal carbide such as MC, M₂₃C₆, M₆C, M₇C₃, or intermetallics. An increase in the oxygen may indicate oxide inclusion. It is reported that in superalloys precipitates generally occur as γ' , η , γ'' , δ , MC, M₂₃C₆, M₆C, M₇C₃, M₃M₂, MN, μ , and σ phases [15].

3.3. Microhardness Test Results

Microhardness measurement was carried out on the base metals, HAZ and, weld metal for determining hardness. The hardness profile obtained is shown in Figure 5.

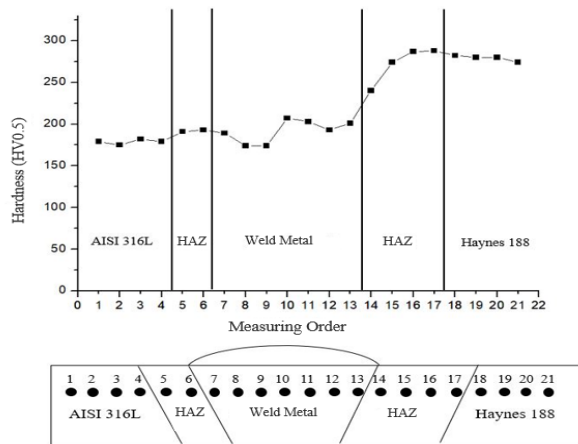


Figure 5. Haynes 188 – AISI 316L weldment microhardness profiles

As seen in Figure 5, the hardness of HAZ on both sides of the welded sample are higher than both base metals in relation to thermal cycling. It is seen that the highest hardness value in the dissimilar metal's weldment is an average of 288HV0.5 in the HAZ of Haynes 188 superalloy. AISI 316L base metal hardness is measured as 178HV0.5 on average. The welded sample hardness shows an increase in the transition from AISI 316L to Haynes 188 depending on different metals properties. It has been determined that the hardness of the weld metal obtained autogenously is 191HV0.5 on average, closer to the that of the AISI 316L main metal. The dilution of the weld metal due to the mixture of AISI 316L and Haynes 188 superalloy in the weld pool during the autogenous welding operation and structural transformation in the weld metal is thought to be the reason for the decrease in hardness of the weld metal.

3.4. Microstructure Results

Macro and microstructure images of the sample prepared from Haynes 188 – AISI 316L weldment, which was welded autogenously with a Force TIG welding machine, are shown in Figure 6 and Figure 7, respectively.



Figure 6. Haynes 188 - AISI 316L weldment macrostructure image.

There has not been any welding discontinuity such as undercut, porosity, insufficient penetration, and solidification cracks in the macrostructure of dissimilar metals weldment (Figure 6). This indicates that it was successfully welded with the Force TIG welding machine, autogenously, without a weld groove.

When the HAZ of the dissimilar metals weldment is examined, it is determined that the Haynes 188 side is wider (300 μ m) due to its lower heat transfer coefficient. The heat transfer coefficient of AISI 316L stainless steel is 113 BTU-in/hr-ft²-°F, while the heat transfer coefficient of Haynes 188 superalloy is 72 BTU-in/hr-ft²-°F [16,17]. The heat in the weld pool diffuses towards to the AISI 316L stainless steel main metal, which has a higher heat transfer coefficient compared to the Haynes 188 superalloy, during the welding process so causes narrower HAZ.

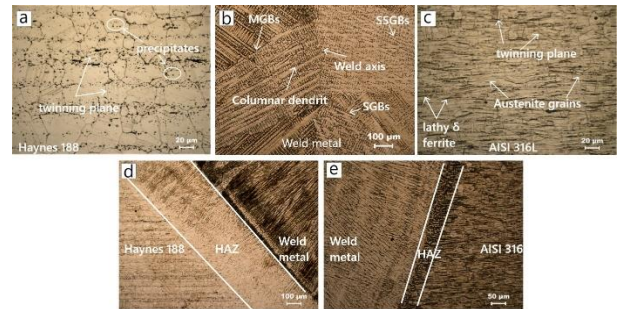


Figure 7. Haynes 188 – AISI 316L dissimilar metals weldment microstructure images, a) Haynes 188 main metal b) Weld metal c) AISI 316L main metal d) HAZ of Haynes 188 e) HAZ of AISI 316L (Solidified grain boundaries (SGBs), Solidified sub-grain boundaries (SSGBs), Migrated grain boundaries (MGBs))

Haynes 188 base metal is composed of grains with a face center cubic lattice structure (Figure 7a). The twinning plane is witnessed in the structure. There are also precipitates thought to be intermetallic and metal carbide phases in grain and at the grain boundaries. Similarly, it has been reported that MC, M₂₃C₆, M₆C, and M₇C₃ carbide precipitate in the structure of cobalt base superalloys [15,18].

In the weld metal in Figure 7b, typical columnar dendritic grains grow parallel to the weld center from the fusion border on both sides of the dissimilar weld metal. The microstructure of the weld metal was solidified entirely austenitic and remained austenitic during cooling to room temperature. Dendritic and cellular structure is seen in primary austenitic solidified microstructures due to separation of alloy and impurity elements during solidification and their relatively low diffusion at high temperature.

The microstructure image of AISI 316L main metal in Figure 7c shows that banding due to deformation and twinning planes in some austenite grains occurred. In addition, some ferrite phase stringers were observed at grain boundaries besides fine equiaxed austenite grains [19].

As mentioned earlier, the Haynes 188 HAZ of the dissimilar welded joint was significantly wider than the AISI 316L stainless steel HAZ (Figure 7d). The taken image nearby the fusion line of AISI 316L HAZ of

dissimilar weld metal was also be decorated by the skeletal type of delta ferrite (Figure 7e).

SEM examination was carried out to evaluate the microstructure of dissimilar metals welded sample, especially the weld metal and heat affected zone regions in detail. The microstructure image is shared in Figure 8

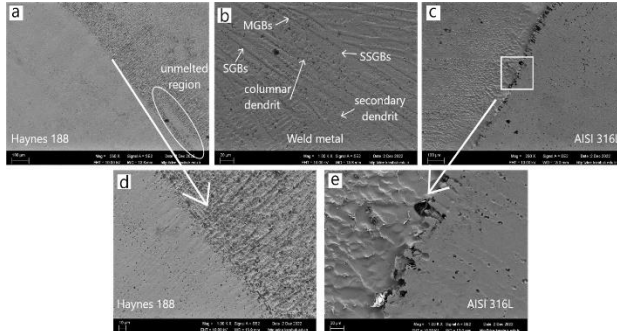


Figure 8. Haynes 188 - AISI 316L dissimilar weldment SEM images, a) Haynes 188 fusion line 250x b) Weld metal 250x c) AISI 316L fusion line 250x d) Haynes 188 fusion line 1000x e) fusion line 1000x (Solidified grain boundaries (SGBs), Solidified sub-grain boundaries (SSGBs), Migrated grain boundaries (MGBs)).

HAZ microstructure images of Haynes 188 and AISI 316L are shown in Figure 8 a and c. The grain growth in the coarse grain region of HAZ is witnessed from the optical image Fig.7d and e. The AISI 316L stainless steel HAZ grains size were estimated to be bigger than the main metal. It is believed that due to the high heat transfer coefficient of stainless steel compared to Haynes 188 superalloy, the heat generated is transferred over this material, causing more grain coarsening in HAZ. Generally, carbon atoms show higher diffusivity in a solid austenitic matrix, resulting in carbon diffusion from the AISI 316L through to weld metal and to the Haynes 188 HAZ. The diffused carbon atoms can combine with alloying elements such as Cr, Co, Fe, W, and B found in Haynes 188 base material, leading to the formation of carbide in addition to those already present in Haynes 188 base metal. It is seen in Figure 8a and d that the precipitates are higher density. The precipitates shown in the Haynes188 HAZ was beautify with Cr, Ni, Mo, and C. They can be MC , $M_{23}C_6$, M_6C , M_7C_3 carbides or intermetallic.

The dissimilar weld metal/AISI 316L stainless steel interface indicate a higher concentration of the lathy and skeletal ferrite (Figure 8e). As seen optical micrograph, a higher concentration of the lathy and skeletal delta ferrite in AISI 316L HAZ was observed correspondent to the weld root than weld kept (Figure 7 e). The intensity was much higher near the fusion border and reduced as it moved away from it. The skeletal type of delta ferrite also beautifies the image taken near the fusion border (Figure 7e). The interface area of AISI 316 main metal/weld metal after etching with an electrolytic solution is shown in Figure 8e. AISI 316L main metal/weld metal is separated along the fusion boundary. There is some level difference among the weld metal and the AISI 316L main

metal surface. This may be related to the metal loss in the weld cycle when using two different etchants for the microstructure investigation of the dissimilar welded joint. The region of the AISI 316L stainless steel HAZ near the fusion line has a large density of lathy and skeletal δ ferrite. The precipitates should be presumed chrome carbide mainly at the grain boundaries is witnessed in the HAZ region of AISI 316L main metal.

A very narrow bright area can be seen between the weld metal and the Haynes 188 superalloy base metal, as shown in Figure 8d. The region is considered to be an unmixed region due to differences in the melting temperature and chemical composition of Haynes 188 superalloy and AISI 316L base metal. The region indicates slightly grain growth as an effect of the autogenously welding processes.

The weld metal has cellular and columnar grains (Figure 8b). The weld metal mainly shows the solidified grain boundaries (SGBs), solidified sub-grain boundaries (SSGBs), and migrated grain boundaries (MGBs) along with the segregation of the alloying elements present mixed from Haynes 188 superalloy main metal during the autogenously welding process. The weld metal near by the weld centerline comprise of the SGBs, SSGBs, and MGBs, as marked in the SEM image (Figure 8b). It is seen that the columnar grains of dissimilar weld metal solidify dendritic depending on the weld cooling rate. The skeletal type of ferrite phase is significantly concentrated on the austenitic stainless-steel side of the weld metal.

In the SEM examinations in Figure 8, it is thought that the weld metal is not mixed sufficiently homogeneous. Since no filler metal is used in the autogenously welding process in the weld metal, the chemical composition elements will inevitably be diluted due to insufficient homogeneous mixing. In addition, the solidification mode has changed due to the cooling rate difference on both base metal sides and different chemical **Şekil 10.** Maksimum Shear Stress Theory'ye göre emniyet katsayısı (S) compositions related to the dilution (Figure 8b, d, and e). For this purpose, a linear EDS analysis of the dissimilar welded sample from both base metals to the weld metal, including the HAZ regions was performed. The results are shown in Figure 9.

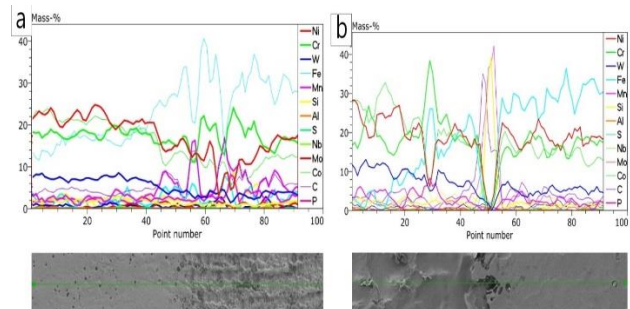


Figure 9. Haynes 188 – AISI 316L fusion line EDS analysis a) Haynes 188 fusion line EDS analysis, b) AISI 316L fusion line EDS analysis.

As can be seen in Figures 9a and b, elemental distribution differences were detected in the transition from both main metals to the weld metal. The elemental distribution ratios obtained as a result of the analysis are given in Table 3, respectively.

Table 3. Compositions of elements of the Haynes188 – AISI 316L dissimilar welded sample (wt.%)

Elements	BM _{H188}	BM _{H188/WM}	WM _{H188}	WM _{AISI316L}	WM _{AISI316L/WM}	BM _{AISI316}
Cr	20.77	16.87	17.24	24.10	17.29	17.21
Fe	2.03	13.57	28.69	9.02	31.15	35.77
Ni	28.18	23.55	16.91	17.93	21.48	21.21
Mo	0.41	0.48	1.25	0.61	1.60	0.99
Mn	3.21	2.40	2.36	3.38	2.78	1.59
Co	29.68	23.65	13.54	22.98	14.87	15.37
W	11.78	8.09	3.44	11.18	0.06	0

In the table, analysis performed areas; Haynes 188 base metal (BM_{H188}), Haynes 188 base metal-weld metal transition line (BM_{H188/WM}), Haynes 188 weld metal side (WM_{H188}), AISI 316L weld metal side (WM_{AISI316L}), Weld metal-AISI316L transition line (WM_{AISI316L/WM}), and AISI 316L abbreviated as base metal (BM_{AISI316L}). The EDS of the dissimilar welded sample emphasized to the concentration of Ni, Cr, Fe, Mo, Mn, Co, and W. When Haynes 188 base metal elemental composition is compared with Haynes 188's HAZ and weld metal side, it is seen that there is an increase in the amount of Fe and a slight diminishing in the amount of W, Ni, Mn, Cr and Co. The elemental change on the weld metal side of HAZ and Haynes 188 is attributed to the rapid and more extensive convection flow occurring at the bottom of the weld pool. This flow results in forming of a thin laminar layer and better mixing of the weld metal and main metal [20]. Since no additional metal was used in this study, there is expected to be a change in composition in the weld metal of the joint because of the mixture of Haynes 188 and AISI 316L.

When the elemental composition of AISI 316L austenitic stainless main metal and HAZ is compared, an almost similar elemental distribution is seen. It is seen that the amount of Fe decreases according to the chemical elemental distribution of the AISI 316L weld metal side, and it is lower than the Haynes 188 side weld metal. This may be related to the metallurgical reaction of the elements in the iron Haynes 188 superalloy, which is abundant in stainless steel, depending on the mixture in the weld pool. Reversibly, a similar increase is observed in the amount of cobalt and chromium on the stainless side of the weld metal. The AISI 316L side can be explained by the influence of Haynes 188 superalloy on the probe of the device, which has a high amount of cobalt in HAZ and its base metal. This elemental variability in the AISI 316L side weld metal indicates that the weld pool is not mixed homogeneously [20–22]. It is reported that when the melting range of the weld metal is similar or higher than main metal, only a small part of the main metal melts completely and re-solidifies without diluting the weld metal [21]. In the SEM examination of the weld metal, small sizes of metal carbides or some intermetallic compounds were observed between the dendrites. Figure 10 shows the EDS analysis results of these precipitates from the weld metal SEM images.

The primary elements shown in the precipitates are, Ni, Co, Fe, Cr, Nb, Mo, Mn, Cu, La, B and W (Figure 10). The carbon and oxygen elements are also indicated in the point analysis. According to the point EDS analysis, the decrease in cobalt, chromium, and tungsten in the precipitates formed in the weld metal, but the significant increase in the amount of carbon and boron in the composition can be shown as evidence of the presence of precipitates. It is presumably a metal carbide such as MC, M₂₃C₆, M₆C, M₇C₃, or intermetallics in a complex composition. It is observed that the precipitates seen in the structure are spherical and quadrangular in form.

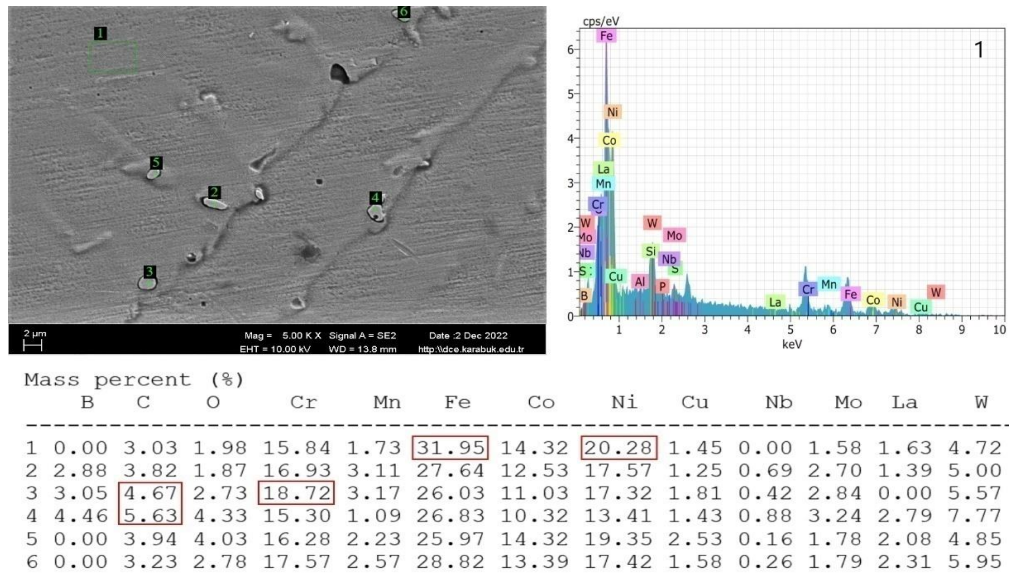


Figure 10. The point EDS analysis results were carried out on the precipitates formed in the Haynes 188 – AISI 316L dissimilar weld metal.

In the literature review, it has been reported that spherical and quadrangular precipitates are carbides formed by metals in the material [23]. Nevcanoglu et al. [24] stated that metal carbides in the chemical forms of TiC, NbC, CrC, and $M_{23}C_6$ in the weld metal of Inconel 718 superalloys joined by TIG welding can affect the material properties positively or negatively depending on their location. Precipitates in austenite grains prevent the movement of dislocations and increase the strength. However, when deposited at the grain boundaries, they become centers that cause stress accumulation and, thus crack formation during deformation. They cause a decrease in fracture toughness and yield-tensile strength. Similarly, Osoba et al. [25] reported that MC carbide precipitates formed in the weld metal and along grain boundaries of Haynes 282 alloy joined by laser welding. It is emphasized by Ferreira. et al. [26], the $M_{23}C_6$ carbides, p , or σ phases are the typical brittle phases that formed dissimilar welding of superalloys and austenite stainless steel. The composition of Cr and Fe in the brittle phases was less than in the grain boundary. Thus they should not be $M_{23}C_6$ carbide [26]. They are probably p or σ phases, in which Mo is enriched, and Ni and Fe are over.

4. GENERAL RESULTS

This study investigated the weldability of Haynes 188 superalloy and AISI 316L austenitic stainless steel, which is preferred in the industry due to their high temperature resistance. The results can be summarized as follow.

- The strength of dissimilar metals weldment, autogenously welded with a Force TIG welding machine,

was higher than that of AISI 316L austenitic stainless steel and lower than that of Haynes 188 superalloy.

- The structure, precipitates, or intermetallic formations and grain size change in the weld metal or due to the metallurgical transformation associated with the thermal welding cycle in HAZ are the reasons for the lower ductility of the welded sample than the base metals.

- The fracture of weldment occurred in ductile mode through the weld metal. In addition, there are precipitates formations or oxide inclusion within the dimples on the fractured surface, which are thought to constitute the fracture initiation.

- The hardness of the welded sample increases as it progresses from the AISI 316L base metal to the Haynes 188 superalloy, depending on the properties of the metals and the structural transformation in HAZ and weld metal. The weld metal hardness of the weldment was determined closer to the hardness of AISI 316L main metal, with an average of 191HV0.5 due to dilution.

- Haynes 188 and AISI 316L base metal, which consists of grains with a face center cubic lattice structure, shows banding due to deformation and twinning plane. In Haynes 188 superalloy, HAZ, and weld metal, there are also precipitates in the grain and grain boundaries. It is presumably a metal carbide such as MC, $M_{23}C_6$, M_6C , M_7C_3 , or intermetallics in a complex composition. The columnar dendritic austenitic grains grow parallel to the weld center from the fusion border of weld metal is witnessed for dissimilar welded samples. The HAZ of the Haynes 188 side of dissimilar metals weldment formed wider due to its lower heat transfer coefficient. The heat transfer coefficient of AISI 316L austenitic stainless steel is higher than the Haynes 188 superalloy. The heat in the weld pool diffuses towards to the AISI 316L stainless steel main metal during the welding process so causes narrower HAZ.

In a conclusion, Haynes 188–AISI 316L dissimilar metals couple can be successfully autogenously welded by using a Force TIG welding machine without weld groove.

ACKNOWLEDGEMENT

Thanks to Mr. Kadir BEYENAL, owner of 2K welding company, for supporting welding equipment in obtaining the welded joint.

FUNDING

This work was supported by the Scientific Research Projects Coordination Unit of Karabük University under the project code number KBU-BAP-22-DR-081. The authors are grateful for their financial support.

DECLARATION OF ETHICAL STANDARDS

The authors of this article declare that the materials and methods they use in their studies do not require ethics committee approval and/or legal-specific permission.

AUTHORS' CONTRIBUTIONS

Ramazan KAÇAR: Performed the experiments and analyse the results.

Samet NOHUTÇU: Performed the experiments and analyse the results.

Hayriye ERTEK EMRE: Wrote the manuscript.

CONFLICT OF INTEREST

There is no conflict of interest in this study.

REFERENCES

- [1] Kaner S., "The effect of aging treatments after TIG welding on AISI 304 stainless steel material on hardness and strength values", *Journal Of Polytechnic*, 24 (4): 1491–1498 (2020).
- [2] Byun T. S., Garrison B. E., McAlister M. R., Chen X., Gussev M. N., Lach T. G., Coq A. Le, Linton K., Joslin C. B., Carver J. K., List F. A., Dehoff R. R. and Terrani K. A., "Mechanical behavior of additively manufactured and wrought 316L stainless steels before and after neutron irradiation", *Journal Of Nuclear Materials*, 548: 1–32 (2021).
- [3] McGuire M. F., "Stainless Steels for Design Engineers", ASM International, 1–304 (2008).
- [4] Reed R. C., "The Superalloys Fundamentals and Applications", *Cambridge University Press*, 1–372 (2006).
- [5] Caiazzo F., Alfieri V., Sergi V., Schipani A. and Cinque S., "Dissimilar autogenous disk-laser welding of Haynes 188 and Inconel 718 superalloys for aerospace applications", *International Journal Of Advanced Manufacturing Technology*, 68: 1809–1820 (2013).
- [6] Dev S., Ramkumar K. D., Arivazhagan N. and Rajendran R., "Investigations on the microstructure and mechanical properties of dissimilar welds of inconel 718 and sulphur rich martensitic stainless steel, AISI 416", *Journal Of Manufacturing Processes*, 32: 685–698 (2018).
- [7] Ahmad G. N., Raza M. S., Singh N. K. and Kumar H., "Experimental investigation on Ytterbium fiber laser butt welding of Inconel 625 and Duplex stainless steel 2205 thin sheets", *Optics And Laser Technology*, 126: 1–10 (2020).
- [8] Henderson M. B., Arrell D., Heobel M., Larsson R. and Marchant G., "Nickel-Based Superalloy Welding Practices for Industrial Gas Turbine Applications", *Science And Technology Of Welding & Joining*, 9 (1): 1–14 (2004).
- [9] Yilbas B. S. and Akhtar S., "Laser welding of Haynes 188 alloy sheet: thermal stress analysis", *The International Journal Of Advanced Manufacturing Technology*, 56: 115–124 (2011).
- [10] Hejripour F. and Aidun D. K., "Consumable selection for arc welding between Stainless Steel 410 and Inconel 718", *Journal Of Materials Processing Technology*, 245: 287–299 (2017).
- [11] Osoba L. O., Ding R. G. and Ojo O. A., "Microstructural analysis of laser weld fusion zone in Haynes 282 superalloy", *Materials Characterization*, 65: 93–99 (2012).
- [12] Ramkumar D. K., Sridhar R., Perival S., Oza S., Saxena V., Hidad P. and Arivazhagan N., "Investigations on the structure – Property relationships of electron beam welded Inconel 625 and UNS 32205", *Materials & Design*, 68: 158–166 (2015).
- [13] Shakil M., Ahmad M., Tariq N. H., Hasan B. A., Akhter J. I., Ahmed E., Mehmood M., Choudhry M. A. and Iqbal, M., "Microstructure and hardness studies of electron beam welded Inconel 625 and stainless steel 304L", *Vacuum*, 110: 121–126 (2014).
- [14] Gope D. K. and Chattopadhyaya S., "Dissimilar Welding of Nickel Based Superalloy with Stainless Steel: Influence of Post Weld Heat Treatment", *Materials And Manufacturing Processes*, 37 (2): 136–142 (2022).
- [15] Geddes B., Leon H. and Huang X., "Superalloys: Alloying and Performance", *ASM International*, Ohio, (2010).
- [16] ASM Matweb, AISI Type 316 Stainless Steel Data Sheet, <https://asm.matweb.com/search/SpecificMaterial.asp?bassnum=MQ316A> (last access date 02.10.2022)
- [17] Haynes International, HAYNES 188 Alloy Data Sheet, http://haynesintl.com/docs/default-source/pdfs/new-alloy-brochures/high-temperature-alloys/brochures/188-brochure.pdf?sfvrsn=bc7229d4_40 (last access date 15.11.2022)
- [18] Akar N. and Çelik F. D. G., "Effect of atmosphere and carbon content on microstructure and mechanical properties of co-cr-mo superalloy dental blocks produced by centrifugal investment casting method", *Journal Of Polytechnic*, 0900 (4): 1435–1446 (2021).
- [19] Kahraman N., Durgutlu A. and Gülenç B., "Investigation of the effect of hydrogen addition to argon shielding gas on weld zone morphology of TIG welded 316L stainless steel", *Journal Of Polytechnic*, 7 (3): 223–228 (2004).
- [20] Cui Y., Xu C. and Han Q., "Effect of ultrasonic vibration on unmixed zone formation", *Scripta Materialia*, 55 (11):

- 975–978 (2006).
- [21] Hua C., Lu H., Yu C., Chen J. M., Zhang M. L. and Li D. Y., "Reduction of Laves phase in nickel-alloy welding process under ultrasonic Ampère's force", *Journal Of Materials Processing Technology*, 252: 389–397 (2018).
- [22] Sirohi S., Pandey S. M., Świerczyńska A., Rogalski G., Kumar N., Landowski M., Fydrych D. and Pandey C., "Microstructure and Mechanical Properties of Combined GTAW and SMAW Dissimilar Welded Joints between Inconel 718 and 304L Austenitic Stainless Steel", *Metals*, 13 (1): 1–17 (2022).
- [23] Nevcanoğlu A., Pazarlıoğlu S. S. and Salman S., "Investigation of Microstructure and Hardness Properties of Inconel 718 Material Combined With TIG Welding After Aging Heat Treatments", *The Internatınonal Conference On Materials Science, Mechanical And Automotive Engineerings And Technology*, 1–7 (2019).
- [24] Nevcanoğlu A., Bozkurt Y. and Salman S., "The Effect of TIG Welding Parameters and Automatization for Non-Heat Treated Inconel 718 Sheets", *Arabian Journal For Science And Engineering*, 46 (12): 12613–12623 (2021).
- [25] Osoba L. O., Ding R. G. and Ojo O. A., "Improved Resistance to Laser Weld Heat-Affected Zone Microfissuring in a Newly Developed Superalloy HAYNES 282", *Metallurgical And Materials Transactions A*, 43 (11): 4281–4295 (2012).
- [26] Ferreira L. D. S., Graf K. and Scheid A., "Microstructure and Properties of Nickel-based C276 Alloy Coatings by PTA on AISI 316L and API 5L X70 Steel Substrates", *Materials Research*, 18 (1): 212–221 (2015).